IEEE Access
Multidisciplinary ⋮ Rapid Review ⋮ Open Access Journal

Received September 8, 2020, accepted November 2, 2020, date of publication November 19, 2020,
date of current version December 8, 2020.

Digital Object Identifier 10.1109/ACCESS.2020.3039457

Projected Performance of InGaAs/GaAs Quantum Dot Solar Cells: Effects of Cap and Passivation Layers

ATIA ISLAM ANKHI[1], MD. RAFIQUL ISLAM[1], (Member, IEEE), MD. TANVIR HASAN[2], (Member, IEEE), AND EKLAS HOSSAIN[3], (Senior Member, IEEE)

[1]Department of Electrical and Electronic Engineering, Khulna University of Engineering & Technology (KUET), Khulna 9203, Bangladesh
[2]Department of Electrical and Electronic Engineering, Jashore University of Science and Technology (JUST), Jashore 7408, Bangladesh
[3]Oregon Renewable Energy Center (OREC), Department of Electrical Engineering and Renewable Energy, Oregon Institute of Technology, Klamath Falls, OR 97601, USA

Corresponding author: Md. Tanvir Hasan (tan_vir_bd@yahoo.com)

ABSTRACT In this work, the effects of $Al_xGa_{1-x}As$ cap and passivation (such as SiO_2, Si_3N_4, and HfO_2) layers on the performance of InGaAs/GaAs-based quantum dot intermediate band solar cells (QDIBSCs) have been studied. The low surface recombination rate of $\sim 10^3$ per cm^3s is achieved by optimizing the composition, $x = 0.40$, and thickness (200 nm) of the $Al_xGa_{1-x}As$ cap layer. The optical reflectance is also evaluated for devices with different passivation. The solar cell with Si_3N_4 shows the lowest reflectance of 10.53%. The photogeneration rate has been enhanced at the quantum dot region because of the improvement of the photocurrent provides by both cap and passivation layers. There is also an increment found in the average external quantum efficiency of 39.56% as compared to that of the bared conventional QDIBSC. As a result, the solar cell, with both $Al_{0.40}Ga_{0.60}As$ cap and Si_3N_4 passivation layers, shows the conversion efficiency of 27.8%, which is higher than that of 21.6% for conventional $In_{0.53}Ga_{0.47}AS$/GaAs-based QDIBSC. These results indicate that GaAs-based QDIBSCs with both $Al_{0.40}Ga_{0.60}As$ cap and Si_3N_4 passivation layers are promising for next-generation photovoltaic applications.

INDEX TERMS QDIBSC, cap layer, passivation, surface recombination rate, photon-generation rate.

I. INTRODUCTION

Photovoltaic (PV) energy becomes more famous for the generation of inexhaustible and renewable electricity leads to help in less the greenhouse effect and contributes to sustainable development. The global PV installation capacity reached $\sim$627 GW_{DC}, which is covered 3% of electricity generation entire countries of the world in 2019 and it is expected to grow by 14%-20% in 2020 from last year [1]. According to International Technology Roadmap for Photovoltaics (ITRPV), developments in all fields of Si-based modules achieve efficiencies of $\sim$20% that will improve to 23%, while the PV cells with heterojunction is expected to attain the module efficiency about 24% until 2030 [2]. Essig *et al.* reported the best research efficiency of 32.8% among all the emerging technology using GaAs/Si tandem solar cell [3]. Si-based solar cells have been controlled the PV markets for many decades due to its availability and environmentally friendly nature [4]. However, the indirect nature of its electronic bandgap is one of the disadvantages of crystalline silicon, rendering it a relatively low absorber of long-wavelength sunlight. Whereas the materials with direct bandgap contribute to optimum design for obtaining exceedingly efficient single or multiple junction solar cells. In recent years, GaAs and its alloy materials have been chosen frequently for solar designing because of their bandgaps cover to the standard spectrum. ALTADEVICES company claimed to have achieved a conversion efficiency record of 29.1% for single-junction, which has created a new step of GaAs-based solar cell [5].

To improve the performance of solar cells beyond the Shockley-Queisser limit, the idea of intermediate band (IB) formation, using quantum dot (QD) has been introduced to achieve high efficiency. It was anticipated that the introduction of QD as an IB in solar cell, the conversion efficiencies of a single p-n junction raise to $\sim$45% in one sun and

The associate editor coordinating the review of this manuscript and approving it for publication was Shuo Sun.

~63% in under full concentration [6]–[8]. The intrinsic layer considers as QDs into p-i-n solar cell to make intermediate band solar cell (IBSC). Generally, III-V materials like GaAs, InAs, InGaAs, etc. are the choice for QDs [9]–[11]. Sugaya *et al.* reported that there were no dislocations observed even after the 400 stacking of $In_{0.4}Ga_{0.6}As$ QD layers and the circuit current density, J_{sc} as well as the conversion efficiency improved with increasing the number of QD layers [11]. In our previous study [12], [13], we focused on only the characteristics of electron wave function with respect to dot-to-dot spacing ($S = S_x = S_y = S_z$ along with the coordinate axes) and size of QD ($L = L_x = L_y = L_z$) for $In_{0.53}Ga_{0.47}As$/GaAs-based QDIBSC [12]. A shift is observed both in IB and density of states due to change in dot spacing, S while the extension of QD size introduces a second IB. We also suggested the possibility of conversion efficiency enhancement due to the creation of multiple IBs. The optimum values of L and S are found as 5 nm and 2.5 nm, respectively [12], [13]. Despite the potential for achieving high performance, though QDIBSC does not exceed the Shockley-Queisser limit, still a large discrepancy is observed between the theoretical and experimental outcomes.

There are many losses have been incorporated with the degradation of efficiency in QDIBSC. Both the non- radiative recombination and reflection of photogenerated charge carriers on the cells' inevitable surfaces are the leading causes of the degradation. There are several reports on the incorporation of cap layer with different names as top layer, epitaxy layer, window layer, passivation layer etc. The carrier recombination loss reduces at the surfaces of Si wafer due to introduction of the heterojunction technology employing amorphous Si as the passivation layer [14]. Bhattacharya *et al.* reported the incorporation of front and back surface passivation layers to diminish recombination losses induced by lateral current flow with the 31% power conversion efficiency of Si-based solar cell [4]. Glunz *et al.* reported that SiO_2 passivation layer played an essential role in Si-based solar cells with the efficiency >20% because of its electrical properties which reduce the surface recombination loss [15]. Bernal-Correa *et al.* and KC *et al.* reported that the $Al_xGa_{1-x}As$ thin film with large bandgap used on top of the GaAs surface showed significant improvement in cell efficiency [16], [17]. However, the detailed understanding of non- radiative recombination and reflection of photogenerated charge carriers on the GaAs-based QDIBSC surface are still inadequate. There is room for material and structural changes to proper inclusion of these issues. Therefore, to clarify these effects on the performance of InGaAs/GaAs based QDIBSC are immensely important.

In this work, InGaAs/GaAs based QDIBSCs have studied in a schematic approach to understanding the effects of both cap and passivation layers on the cell performance. QDIBSCs are reintroduced with the surface cap layer to deter the unwanted recombination of photogenerated electron-hole pairs. The crystalline parameters of GaAs and $Al_xGa_{1-x}As$ indicates almost similar properties. The aim of choosing the composition x of $Al_xGa_{1-x}As$ as a cap layer is to study whether it has any impressive effect on the conversion efficiency of QDIBSC. The thickness of the top $Al_xGa_{1-x}As$ capping layer is determined by evaluating the electrical parameters of the cell. Victoria et at. reported that semiconductors having a high refractive index (n > 3) causes around 30% reflection from the surface of the cell [18]. As the optical reflection decreases the photogeneration and photo-current, the top passivation layer has been studied to lessens the reflectance of the QDIBSC. For keeping the reflectivity low throughout the QD absorption region single-layer SiO_2, HfO_2 and Si_3N_4 are analyzed to determine the suitable passivation material. The external quantum efficiency is also explored at different incident wavelengths. The influence of the cap and passivation layer on the conversion efficiency, open-circuit voltage, short circuit current density and fill factor are studied.

The rest of the paper is organized as follows: Section II demonstrates the entire simulation and modelling. In section III, the results of the simulation have been shown with the necessary illustrations. The effect of both the cap and passivation layer can also be realized from this section. In addition, discussion with adequate explanations has also been provided in this section to comprehend the outcome of the results. Finally, in section IV, the study has been concluded.

II. SIMULATION AND MODELLING

The schematic diagrams employed in the simulation are shown in Figure 1. For only simulating QDIBSC device A (Figure 1(a)), structure is used, then to study the impact of cap layer device B (Figure 1(b)) is considered. In order to demonstrate the effect of passivation layers device C (Figure 1(c)), is considered and using different materials individually as such as SiO_2, Si_3N_4, and HfO_2 as passivation layer devices C1, C2, C3 are explored, respectively. Finally, an optimized device structure having the passivation layer over the cap layer is used in device D (Figure 1(d)). The material parameters and size of QD have picked from our previous reports [12], [13]. The QDIBSC structure consists of $In_{0.53}Ga_{0.47}As$ dots and GaAs barrier material. Moon *et al.* reported the composition $x = 0.53$ of $In_{0.53}Ga_{0.47}As$ dots (corresponding bandgap, $E_g = 0.75$ eV) which embedded with GaAs ($E_g = 1.42$ eV) plays as a barrier for both electron and heavy-holes and as a well for light holes [19]. A stack is considered with ten-layers of QD measuring $5 \times 5 \times 5$ nm^3 and spacing between dot-to-dot is 2.5 nm (inset of Figure 1 (a)) [12], [13]. In the simulation model, n-type GaAs (100) is a substrate, n-GaAs is considered as both buffer and base layer, n-$In_{0.5}Ga_{0.5}P$ BSF layer is Si-doped having a concentration of 1×10^{17} cm^{-3}, and both p-GaAs emitter and p-$Al_xGa_{1-x}As$ cap layers are Mg-doped with a concentration of 1×10^{18} cm^{-3} and 3×10^{18} cm^{-3}, respectively. The thickness of each layer is represented in Figure 1. To maintain low-contact resistivity for devices C and D, combine of p+ GaAs with a doping concentration of 1×10^{19} cm^{-3} and Au having a resistivity of 2.35 $\mu\Omega$-cm are considered as

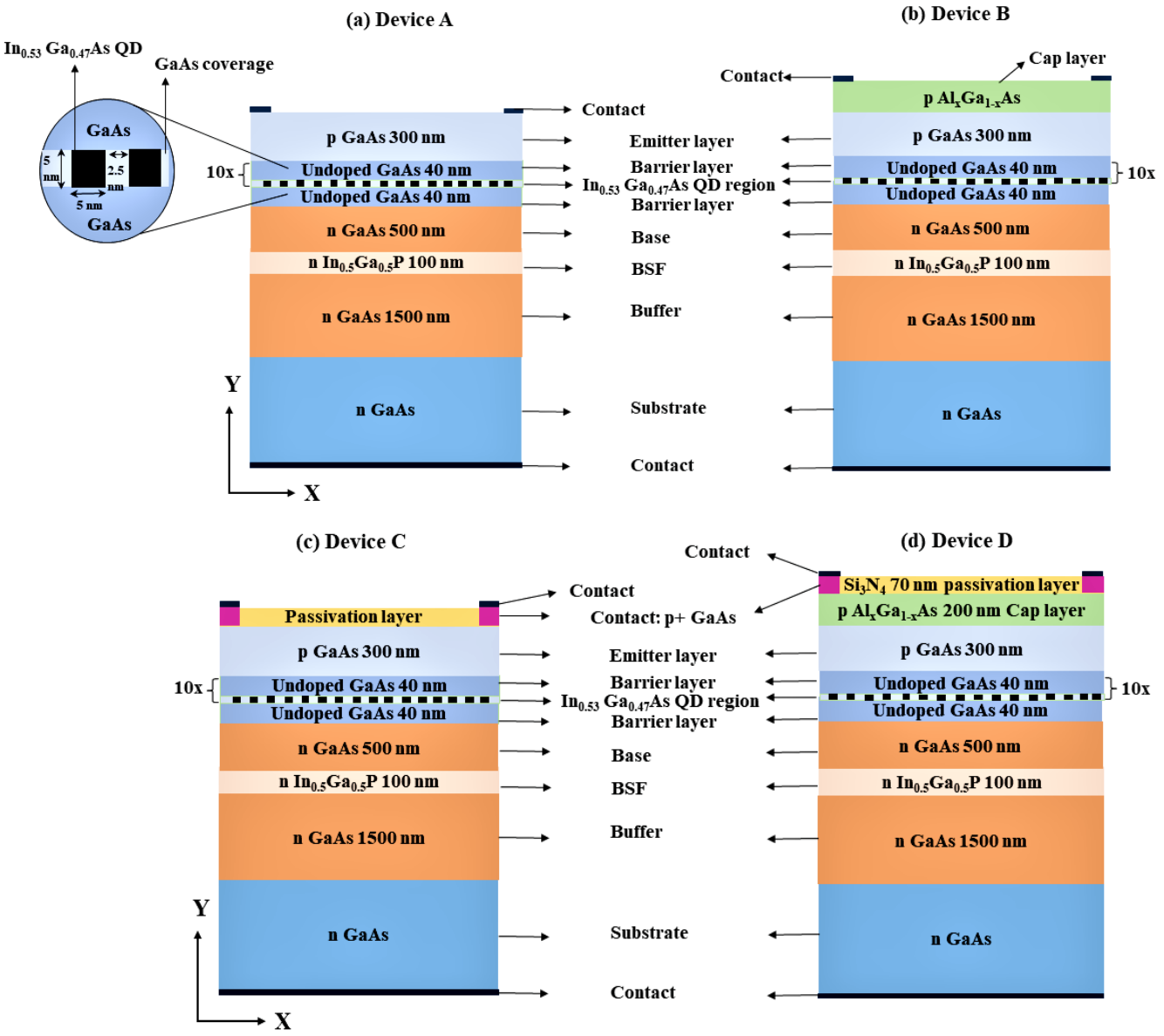

FIGURE 1. Schematic cross-sectional views of the QD solar cell employed in this simulation (a) device A, (b) device B, (c) device C, and (d) device D.

a contact. However, only Au with the same resistivity is employed for devices A and B, which have no passivation layer.

The total dimension of the cell is 1 × 0.1 mm^2. These device structures are simulated using the Silvaco ATLAS platform. All the simulations have done under 1 sun with a normal-incident light source, and at room temperature (300K).

The structures of the solar cell are specified by the mesh, region, electrodes, and doping rates. Different types of models are employed to simulate the structures. The time-independent Schrodinger equation and the Kronig-Penney model are considered to explain the wave function of the electrons in dots and barriers. The Schrodinger equation for a single electron in a QD array can be represented as [20], [21]

$$\left[-\frac{\hbar^2}{2}\nabla_r\frac{1}{m_r^*}\nabla_r + V(r)\right]\varphi(r) = E_\varphi(r) \tag{1}$$

where, $E_\varphi(r)$ is the total energy, the potential, $V(r) = Vx(x) + Vy(y) + Vz(z)$, is the sum of the total potential along with the x, y, and z axes, respectively, and $\phi(r)$ is the envelope of wave functions. The $\hbar = h/2\pi$, h is the Planck's constant. Equation 1 has been solved the Kronig-Penney model. The formation of IB in the QD region is shown in Figure 2. Shockley-Read-Hall, Auger, Surface recombination models are employed to study the effectiveness of the cap layer. After inputting the physical parameters of the constituent materials,

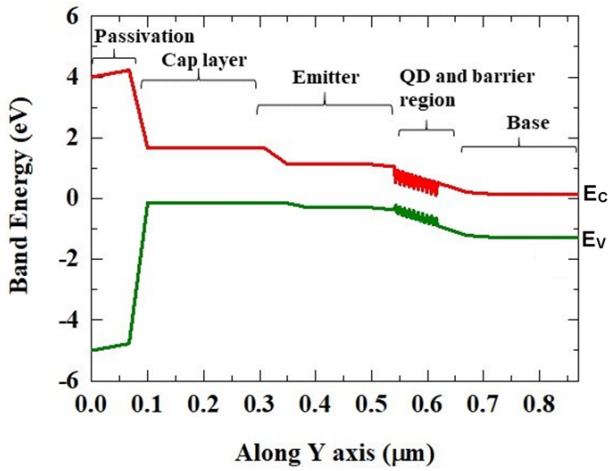

FIGURE 2. Schematic energy band diagram of the device D.

numerically analyzed the solar cell's electrical and optical characteristics.

The criteria of a suitable cap layer for a solar cell, the material have to show three essential features [22], [23]. Firstly, the material should have a higher bandgap as compared to the active material of the solar cell; else, the photons having suitable energy will be absorbed by the cap layer. Secondly, the lattice mismatch should be minimum between the capped and active materials to attain the excellent crystalline quality. Lastly, the cap layer must be capable of reducing the surface recombination velocity of the cell through the introduction of an energy barrier to increase the electron-hole pair generation by lessening the dangling bonds density at the interface. From Figure 2, it indicates that $Al_xGa_{1-x}As$, as a suitable candidate for cap layer, possess large tunable bandgap (1.42 - 2.16 eV) regarding the consecutive surface of GaAs (E_g = 1.42 eV). The maximum lattice mismatch between GaAs and $Al_xGa_{1-x}As$ is less than 0.15%, which is very low to produce good quality crystal. The surface recombination rate is calculated to conclude the effect of $Al_xGa_{1-x}As$ as a cap layer. The optimization, in terms of both composition of x and thickness of the cap layer, is performed to achieve high conversion efficiency.

The refractive index is one of the critical parameters to determine the optical properties of the solar cells. It is expressed as [24]

$$n_i = n_o^{\frac{N-i+1}{N+1}} n_l^{\frac{i}{N+1}} \tag{2}$$

where i refers to the ith layer of passivation, N corresponds to the number of the passivation layer on the surface, $n_o$and n_l imply to the refractive index, n of the air and GaAs surface, respectively. The reported value of n is ∼4.06 for GaAs at the wavelength, λ = 550 nm [25]. According to equation (2), for a single passivation layer (N = 1) on device A, the value of the calculated optimum n is 2.01. Some materials such as SiO_2, Si_3N_4, and HfO_2 having a n of 1.46, 2.04, and 2.11 at λ = 600 nm, respectively. These results indicate that the Si_3N_4 might be the most suitable material for passivation layer because of its n near to the theoretical optimal value of n = 2.01. Further simulation is conducted to study the optimum material and thickness of the passivation layer for device C.

The anti-reflection property of SiO_2, Si_3N_4, and HfO_2 as passivation material is analyzed to observe its effect on the performance of device C1, C2, and C3, respectively. The photo absorption and photogeneration rates help to understand the effect of both cap and passivation layer on device D. The photogeneration rate (G) is governed by the equation (3) [21],

$$G = \eta_0 \frac{P\lambda}{hc} \alpha e^{-\alpha y} \tag{3}$$

where, η_0 and P are defined as the internal quantum efficiency and ray intensity factor, respectively. The P consists of transmissions, reflections, and loss due to absorption over the photo ray path. Also, y and α are the relative distance of the photo ray and absorption coefficient, respectively. Usually, α depends on the optical constant of a material. The net photocurrent and external quantum efficiency have also calculated using the Refs. [21], [26].

We have reproduced experimental reported results using our simulation models to compare those data for validity test purpose. The fabricated InAs/GaAs based QDSC structure is considered with the same material parameters and dimension of the cell [27]. There is a good match between the experimental and our simulated data, as shown in Figure 3. These results indicate evidence of the validity of our simulation models.

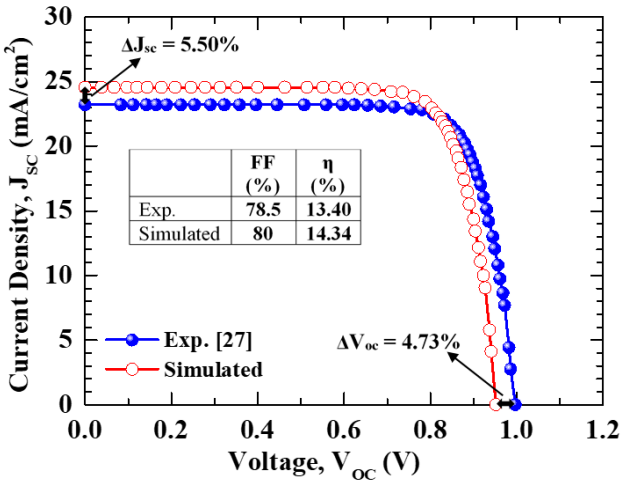

FIGURE 3. Model validation by comparing with experimental results.

III. RESULT AND DISCUSSION

The short circuit current density-open circuit voltage, J-V characteristics of device A are shown in Fig. 4, under dark and illumination conditions. The values of J_{sc} and V_{oc} are 31.56 mA/cm^2 and 0.876 V, respectively under one sun. As a

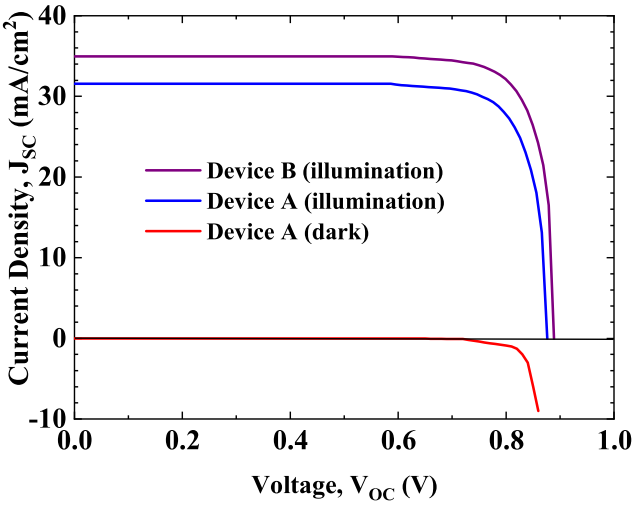

FIGURE 4. J-V characteristics of device A under illumination and dark conditions and device B under illumination.

result, the conversion efficiency, η is calculated as of 21.6% with a fill-factor, FF = 80%. In order to have more conversion efficiency both J_{sc} and V_{oc} need to be increased. Therefore, additionally, cap and passivation layer on the top surface of device A is included to study their effectiveness.

A. EFFECT OF CAP LAYER

In device B, an additional cap layer consists of $Al_xGa_{1-x}As$, which is considered on top of device A to enhance the performance, as shown in Fig. 1 (b). Figure 4 shows the effects of the cap layer on both J_{sc} and V_{oc} of device B over the J-V characteristic of device A. The values of J_{sc} and V_{oc} are 34.96 mA/cm^2 and 0.889 V, respectively. The J_{sc} enhances ∼10% by introduction of $A_xlGa_{1-x}As$ cap layer due to the possible reduction of the recombination rate at the surface of device A. The dangling bonds on the surface of GaAs act as the recombination trap centers. The $A_xlGa_{1-x}As$ helps to destroy bonds with the surface charges leading to enhance the J_{sc} due to increase the electron-hole pair generation rates. The recombination rates represent using contour plots for both devices A (a) and B (b), as shown in Fig. 5. A high surface recombination rates of $\sim 10^{16}$ - 10^{23} per cm^{3}s are found around the QD surfaces of device A as shown in Fig. 5 (a). However, the device B shows the lower recombination rates as $\sim 3 \times 10^3$ per cm^{3}s as compared to that ($\sim 10^{16}$ per cm^{3}s) of device A. These results indicate that carrier recombination rates reduce because of $A_xlGa_{1-x}As$ which interacts with the surface charges leading to eliminate the dangling bonds. Therefore, the effects of Al composition, x and thicknesses of $A_xlGa_{1-x}As$ cap layer on device performance have been shown.

As the lattice matching and bandgap engineering are the essential issues for designing of a high-efficient solar cell, the Al composition, x of $Al_xGa_{1-x}As$ is varied from 0 to 1. The effects of x on the J_{sc} and V_{oc} are shown in Fig. 6. There is no significant change found for V_{oc} after $x = 0.1$. However, two peaks, $x = 0.4$ and 0.8, are obtained for J_{sc} with the values of 34.65 mA/cm^2 and 33.92 mA/cm^2, respectively. These results indicate that $Al_xGa_{1-x}As$ with $x = 0.40$ is the suitable candidate due to low lattice mismatch of 0.025% with

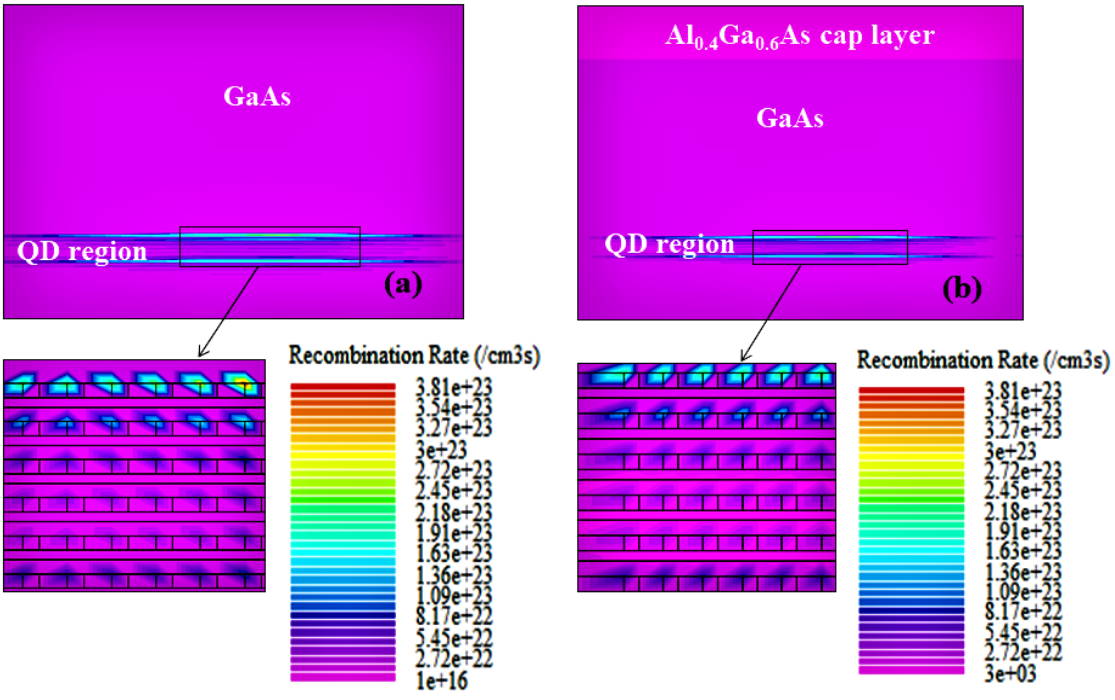

FIGURE 5. Recombination rates of (a) device A and (b) device B.

GaAs and chemically less oxidation sensitivity as compared to $Al_{0.80}Ga_{0.20}As$. Besides these, it has a bandgap of 1.92 eV, at $x = 0.40$, which is higher than that ($E_{GaAs} = 1.42$ eV) of the GaAs surface. As a result, the optimum x is considered as 0.40 for the next following steps.

The thickness of $Al_{0.40}Ga_{0.60}As$ cap layer has varied from 0 to 500 nm for optimizing the performance of device B, as shown in Fig. 7. Figure 7 (a) shows that the J_{sc} increases with the subsequent increment in $Al_{0.40}Ga_{0.60}As$ thickness because the recombination rate at the surface gets lower as compared to device A. Thus, the interface between $Al_{0.40}Ga_{0.60}As$ cap layer and GaAs surface reflect minority carriers while allowing majority carriers, thus leads to an increment in the collection of current during the short circuit. The V_{OC} remains almost unchanged with the increment of cap layer thickness. From Figure 7 (b), it is noticed that the FF increases with thickness and shows a maximum of 81.3% at 200 nm. With the further increase in thickness, FF reduces due to the possible reason for the enhancement of the series resistivity, which is not considered for simplicity. However, conversion efficiency becomes a maximum of the value of 25.91% at 200 nm thickness. If the increment of thickness keeps on above 200 nm, few of photons will be started to absorb by the active layer. Hence, 200 nm is considered as an optimized thickness of the $Al_{0.4}Ga_{0.6}As$ cap layer.

B. EFFECT OF PASSIVATION LAYER

The optical reflection is another primary reason to reduce the photogeneration and photo-current of the solar cell. Different passivation materials have studied to get rid of this problem. The passivation materials employ top of device A, which is newly defined device C, as shown in Fig. 1 (c). Three kind of dielectric materials, such as SiO_2 ($\varepsilon_r = 3.9$), Si_3N_4 ($\varepsilon_r = 7.5$), and HfO_2 ($\varepsilon_r = 22$) are considered as passivation, which are mentioned as devices C1, C2, and C3, respectively [21]. It is found that the devices (C1, C2, and C3) show higher value of J_{sc} as compared to that of device A (34.96 mA/cm^2). However, the V_{oc} remains almost constant (0.889 V) by replacing passivation materials, as shown in Fig. 8 (a). The η (Fig. 8 (b)) of devices C1, C2, and C3 have been dominated through the J_{sc} leading an improve by ~16.4% as compared to bared device A. The graphical representation of external quantum efficiency (EQE) in Fig. 8 (c) indicates that device C2 has a slightly higher EQE as compared that of other devices C1 and C3. There is a variation found in J_{sc} due to different passivation materials as represented in Fig. 8 (a). as well as the reflection of these changes, has been replicating on both η and FF (Fig. 8 (b)). Mainly, optical reflection plays a vital role in solar cell performance, and passivation materials help to reduce the reflectivity. The reflection spectra of devices A, C1, C2, and C3 represent (Fig. 9) in the spectral region of 300-1200 nm. These results indicate that the optical reflection losses of the QDIBSC structure reduce because of the passivation layer.

This passivation minimizes the reflectivity of the GaAs surface and increases the absorption of the photons. In Fig. 9, device A has no anti-reflection layer that causes the high reflectance up to ~800 nm region of the wavelength, λ. On the other hand, the introduction of SiO_2, Si_3N_4, and HfO_2 as passivation materials, which act as an anti-reflection layer, can lower the reflectance as compared with the bared device

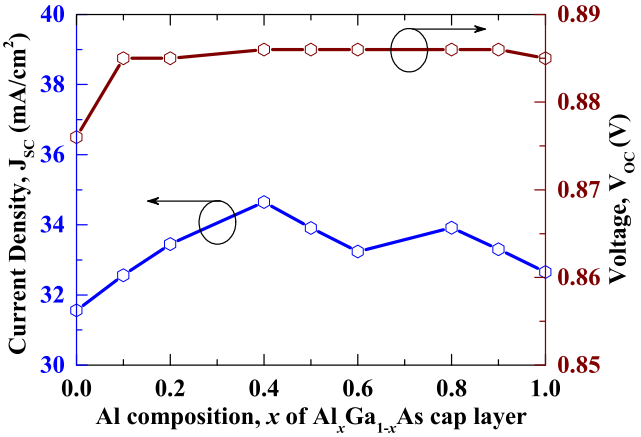

FIGURE 6. Variation in current and voltage for different Al compositions in device B.

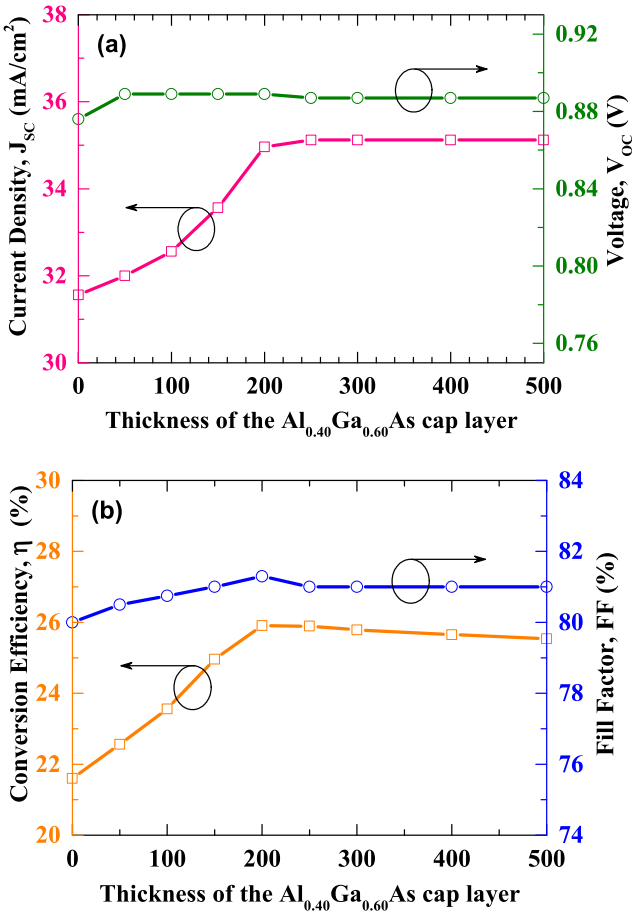

FIGURE 7. The variation in (a) short circuit current density and open-circuit voltage, (b) conversion efficiency and fill factor for different thickness of the $Al_{0.40}Ga_{0.60}As$ cap layer.

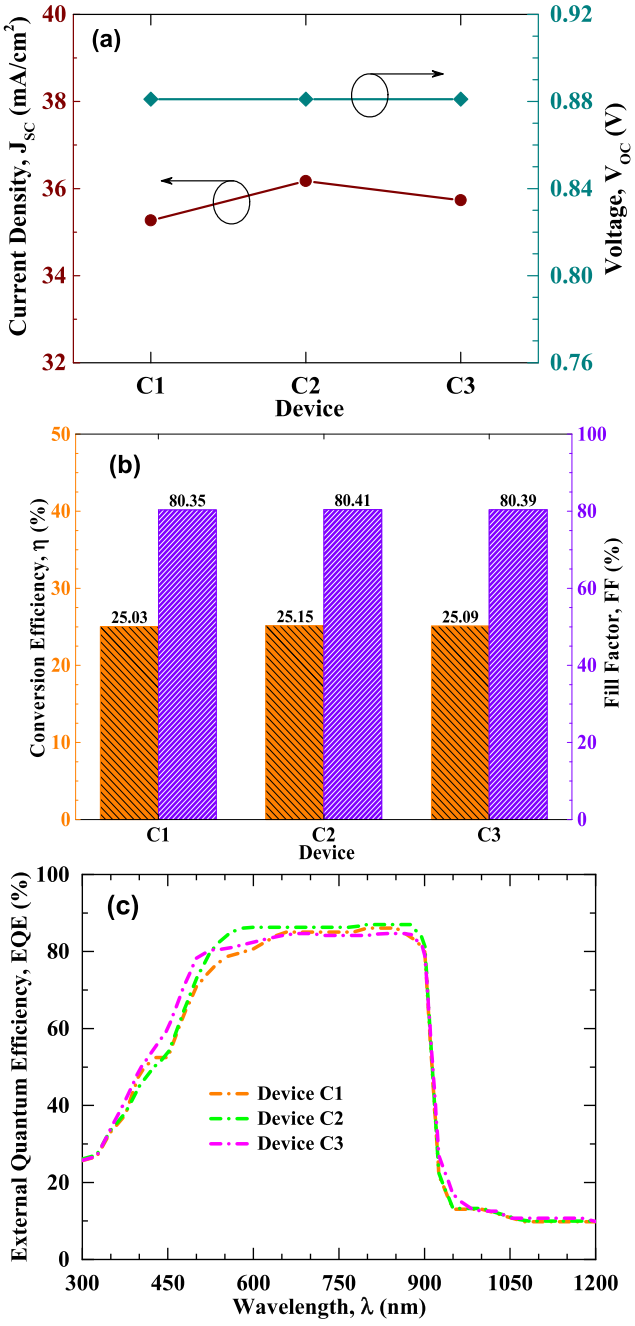

FIGURE 8. Effect of different passivation materials on the performance of device C, (a) short circuit current density and open-circuit voltage, (b) conversion efficiency and fill factor, (c) external quantum efficiency.

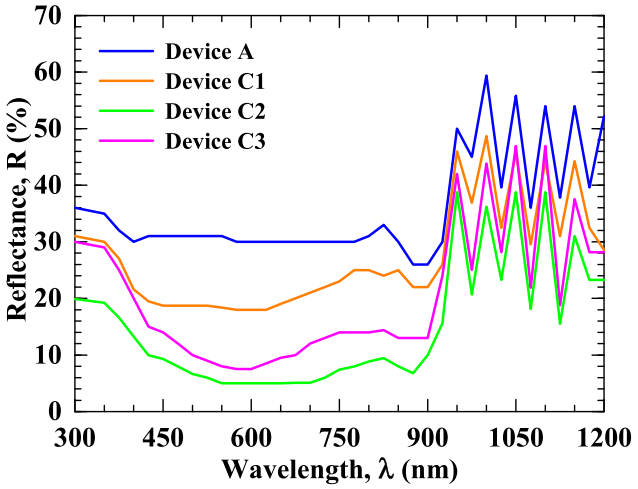

FIGURE 9. Optical reflectance of device A and device C (C1, C2, and C3) with different passivation.

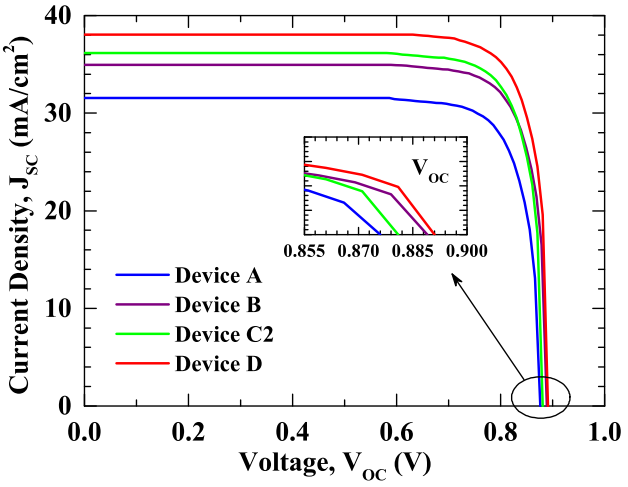

FIGURE 10. J-V characteristics of device D in comparison with devices A, B, C2 under illumination (1 sun).

A. In the region of λ =∼ 800-900 nm, it has comparatively less reflectance than other wavelength regions because the GaAs surface has more absorbance in this region. There is an oscillation seen in λ > 900 nm for all simulated devices. These results elucidate the possibility of an interference effect of the QD layer structure. Moreover, this oscillation may be occurred from the resonance of light at the interface between the consecutive layers and the substrate [29]. There are several reports which have also indicated these similar effects [16], [17]. Thus, the introduction of passivation layer helps to reduce the resonance to lessen reflectance of the devices in the long wavelength range. Furthermore, the reason for having lower reflectance for HfO_2/Si_3N_4 layer is the close matching of the refractive index with the theoretical optimum value. It is found from the Fig. 9 that the device C2 with Si_3N_4 has lower reflectance as compared to that of other simulated devices.

Since the reflectivity value changes with the wavelength, the average weighted reflectance value can be calculated from the simulated results using the following equation (4) [28]

$$R_W = \frac{\int_{350\ nm}^{900\ nm} R(\lambda)\,\phi(\lambda)\,d\lambda}{\int_{350\ nm}^{900\ nm} \phi(\lambda)\,d\lambda}. \quad (4)$$

where R(λ) and $\phi(\lambda)$ are the value of reflectance and photon flux at a specific λ, respectively. The average weighted reflectance (R_W) value of device A is 34.12%. However, with the introduction of passivation, the reflectance value becomes lower for devices C1 (22.6%), C2 (10.53%) and C3 (14.5%) as compared to without passivated device A. These

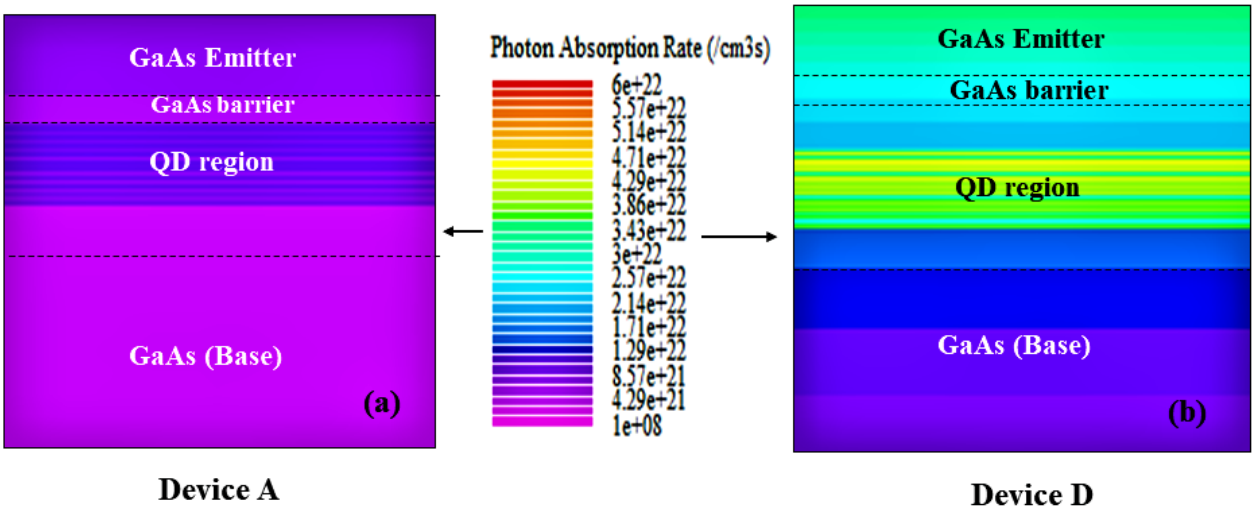

FIGURE 11. Photon absorption rate distribution of device A (a) and device D (b).

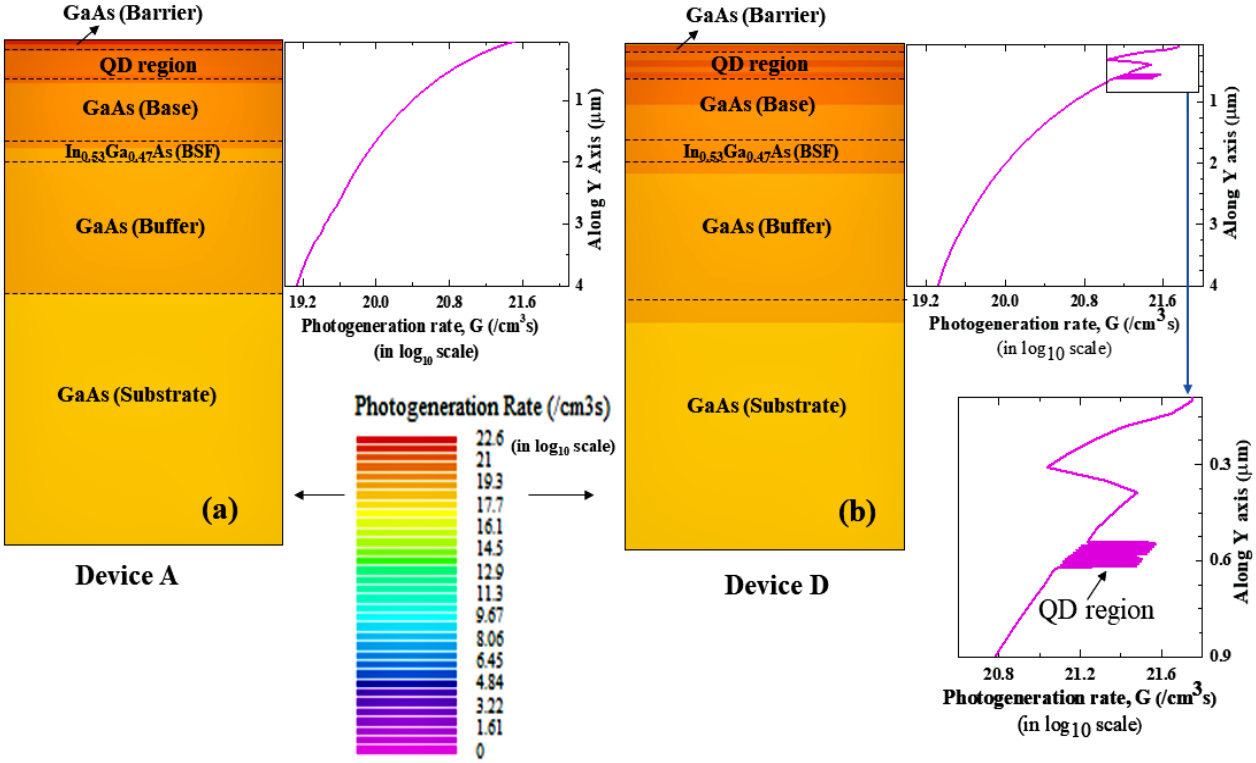

FIGURE 12. Photogeneration rate distribution of device A (a) and device D (b).

results indicate that the optical reflection becomes low by leading to the absorption of more photons to generate more photo-current for providing better performance. The optimization of the passivation's thickness is of great importance to know the efficient cell structure. The optimum thickness can be evaluated from a well-known quarter wavelength rule, $d_i = \lambda/4n_i$. According to this rule, optimum thicknesses for SiO_2, Si_3N_4, and HfO_2 are 94 nm, 70 nm, and 65 nm, respectively. These values are considered for the simulation of devices C1, C2, and C3, accordingly. Hence, it can be concluded that the Si_3N_4 is the suitable passivation materials for high-efficiency solar cells.

C. EFFECT OF BOTH CAP AND PASSIVATION LAYERS

Device D (Fig. 1 (d)), with both optimized cap and passivation layers, has been studied to evaluate the cell performance.

There are improvements found (Fig. 10) in both J_{sc} and V_{oc} of device D as compared to those of device A. The enhanced values of J_{sc} and V_{oc} are 38.04 mA/cm^2 and 0.891 V, respectively. Both photo absorption rate and photogeneration rate play a vital role in increasing the overall cell performance. Figures 11 and 12 show the contour plots of photon absorption and photogeneration rates, respectively, for both devices A and D. The photon absorption rate in the QD and other consecutive regions get increased in device D (Fig. 11 (b)) as compared to device A (Fig. 11 (a)) due to the inclusion of both cap and passivation layers. There is also a significant increment in photogeneration rate at the QD region of the device D (Fig. 12 (b)) than that of device A (Fig.12 (a)). These results indicate that the increment of the photon absorption rate accelerates the process of photogeneration rate leading to the considerable improvement of the photocurrent provides by both cap and passivation layers in device D. Moreover, this photocurrent is considered as the dominant reason for the increment in the open-circuit voltage and fill factor.

The EQE has great importance for observing the effect of the cap layer and passivation layer on a solar cell's performance. The EQE of each structure has been evaluated, which is shown in Fig. 13. Device B's quantum efficiency shows promising results in 600-850 nm wavelength, whereas device C2 has a wider 525-850 nm wavelength region with maintaining a little high EQE. However, it shows a very high EQE in a broad region of wavelength from 500- 850 nm for device D due to both recombination and antireflection mechanisms induced from cap and passivation layers. These cap and passivation layers lead to absorb a wide range of photons from 500-850 nm by decreasing the optical reflection losses. Since EQE value changes with the wavelength, the average weighted EQE value can be calculated from the simulated results with the equation (5), as follows [29]:

$$EQE_W = \frac{\int_{300\ nm}^{900\ nm} EQE\ (\lambda)\ \phi\ (\lambda)\ d\lambda}{\int_{300\ nm}^{900\ nm} \phi\ (\lambda)\ d\lambda} \tag{5}$$

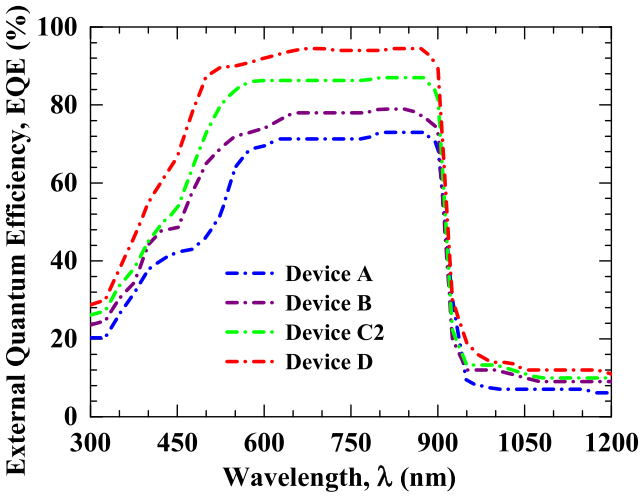

FIGURE 13. EQE response of device A, device B, device C2, and device D.

where, EQE (λ) and ϕ (λ) are the external quantum efficiency and photon flux at a specific wavelength (λ), respectively. The average external quantum efficiency, EQE_W are 15.47%, 31.63%, and 39.56% for devices B, C2, and D, respectively, from the bared conventional QDIBSC (device A). As a result, the increase in the net photocurrent gives rise to conversion efficiency.

Figure 14 (a) shows a clear view of the change of J_{sc} and V_{oc} according to different device structure. The increment of J_{sc} in devices B, C2, and D are 10.77%, 14.61% and 20.53%, respectively than that of device A. There is slight increment of V_{oc} valued 1.48%, 0.57% and 1.71% in devices B, C2, and D, respectively than that of device A. The reduction of both surface recombination rate and optical reflectivity lead to enhance the J_{sc}. From the overall simulation results, it is found that V_{OC} and FF are slightly increased with the incorporation of cap and passivation layers in device D structure. As the value of J_{sc} increases, the V_{OC} also increases. The value of FF increased with the decrement in surface recombination rate and the improvement in photogeneration rate. According to the above analysis, it is clear that the structure of device D is the most promising for future QDIBSC structure. The electrical output parameters of the simulated solar cells are summarized in Table 1. The comparison of the performance of our simulated device D with others reported device structure is shown in Table 2.

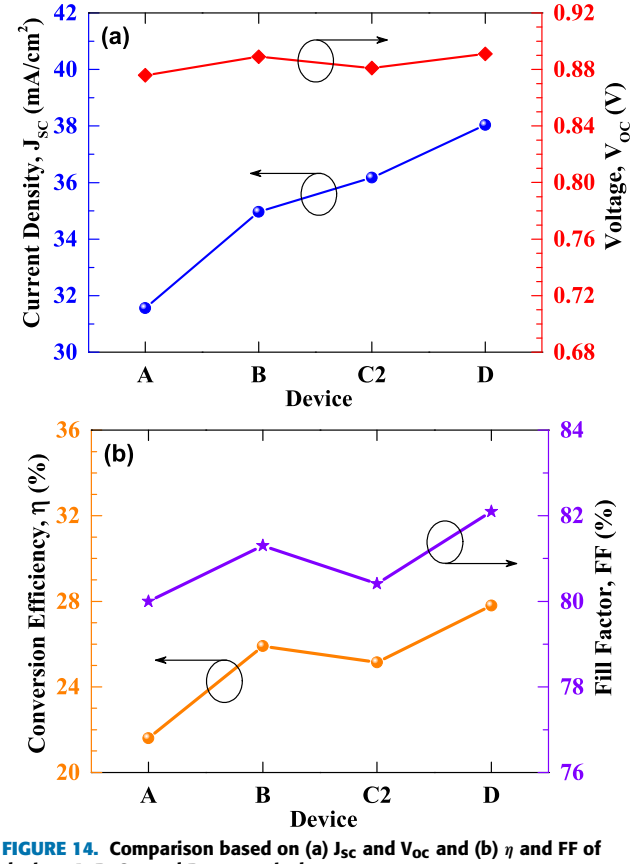

FIGURE 14. Comparison based on (a) J_{sc} and V_{oc} and (b) η and FF of devices A, B, C2, and D, respectively.

TABLE 1. Electrical output parameters of the simulated solar cells.

Solar cell	J_{sc} (mA/cm^2)	V_{oc} (V)	FF (%)	η (%)
Device A	31.56	0.876	80	21.6
Device B	34.96	0.889	81.3	25.91
Device C2	36.17	0.881	80.41	25.15
Device D	38.04	0.891	82.1	27.8

TABLE 2. Comparison between different types of the solar cell with our simulated one.

Classification		J_{sc} (mA/cm^2)	V_{OC} (V)	FF (%)	η (%)
Passivated	HJ-IBC [14]	42.30	0.744	83.80	26.30
	poly-Si/SiOx passivated contact with a SiNx capping layer [30]	38.88	0.618	79.85	20.85
	Poly-Si passivating contacts IBC [31]	38.00	0.673	75.20	19.20
	SiOx flim on Topcon Solar cell [32]	NA	0.687	81.09	22.43
	SiO_2 AR coating on monocrystalline silicon cell [37]	37.77	0.621	77.58	17.80
	HfO_2 layer on heterojunction c-Si Solar cell [38]	38.75	0.724	74.90	21.00
p-n GaAs	Single-Junction [19]	27.06	0.980	83.35	22.08
p-i-n	p-i-n GaAs [33]	20.00	0.620	74.70	9.09
	Double heterojunction [34]	3.31	2.260	84.60	6.43
	AlGaAs/Si dual-junction tandem solar cell [39]	11.90	1.630	65.00	12.70
QDIBSC	InGaAs/GaAs QDIBSC with a light scattering rear texture [35]	21.50	0.760	75.10	12.20
	Capping on InAs/GaAs QD [36]	24.40	0.998	82.00	20.00
	InGaAs/GaAs QIBSC [12] (our previous works)	32.05	0.886	80.30	22.80
	This work	**38.04**	**0.891**	**82.10**	**27.80**

IV. CONCLUSION

The $In_{0.53}Ga_{0.47}As$/GaAs QDIBSC's structure has been optimized by both cap and passivation layers to reduce surface recombination and reflectance rates. The device with 200 nm $Al_{0.40}Ga_{0.60}As$ cap layer shows a low recombination rate of 3×10^3 per cm^{3}s. Results reveal that the employ of 70 nm thick Si_3N_4 passivation decreases the reflectance by improving the whole-cell photogeneration rate. Therefore, the overall efficiency of device D has increased from 21.6 % to 27.8% with the increment of short circuit density from 31.56 mA/cm^2 to 38.04 mA/cm^2 along with a minimal open circuit voltage increment of 15 mV by using both cap and passivation layers on the top of device A. Thus, the concept of introducing capping and passivation on the surface may help the growth engineer to overcome the short-coming of low conversion efficiency in QDIBSC.

REFERENCES

[1] D. Feldman and R. Margolis. (May 28, 2020). *NREL Reports: Q4 2019/Q1 2020 (Solar Industry Update)*. Accessed: Sep. 8, 2020. [Online]. Available: https://www.nrel.gov/research/publications.html

[2] (Apr. 2020). *International Technology Roadmap for Photovoltaic (ITRPV): 2019 Results, Eleventh Edition*. Accessed: Sep. 8, 2020. [Online]. Available: https://itrpv.vdma.org/web/itrpv/download

[3] S. Essig, C. Allebé, T. Remo, J. F. Geisz, M. A. Steiner, K. Horowitz, L. Barraud, J. S. Ward, M. Schnabel, A. Descoeudres, D. L. Young, M. Woodhouse, M. Despeisse, C. Ballif, and A. Tamboli, "Raising the one-sun conversion efficiency of III–V/Si solar cells to 32.8% for two junctions and 35.9% for three junctions," *Nature Energy*, vol. 2, no. 9, p. 17144, Aug. 2017, doi: 10.1038/nenergy.2017.144.

[4] S. Bhattacharya and S. John, "Beyond 30% conversion efficiency in silicon solar cells: A numerical demonstration," *Sci. Rep.*, vol. 9, no. 1, Aug. 2019, Art. no. 12482, doi: 10.1038/s41598-019-48981-w.

[5] *Efficiency Record Isn't the Biggest Change for Alta Devices' GaAs Solar Technology*. PV Mag. Accessed: Sep. 8, 2020. [Online]. Available: https://www.pv-magazine.com/2018/12/17/efficiency-record-isnt-the-biggest-change-for-alta-devices-gaas-solar-technology/

[6] A. Luque and A. Martí, "Increasing the efficiency of ideal solar cells by photon induced transitions at intermediate levels," *Phys. Rev. Lett.*, vol. 78, no. 26, pp. 5014–5017, Jun. 1997, doi: 10.1103/PhysRevLett.78.5014.

[7] G. Wei, K.-T. Shiu, N. C. Giebink, and S. R. Forrest, "Thermodynamic limits of quantum photovoltaic cell efficiency," *Appl. Phys. Lett.*, vol. 91, no. 22, Nov. 2007, Art. no. 223507, doi: 10.1063/1.2817753.

[8] R. Tamaki, Y. Shoji, Y. Okada, and K. Miyano, "Spectrally resolved intraband transitions on two-step photon absorption in InGaAs/GaAs quantum dot solar cell," *Appl. Phys. Lett.*, vol. 105, no. 7, Aug. 2014, Art. no. 073118, doi: 10.1063/1.4893879.

[9] G. Jolley, L. Fu, H. F. Lu, H. H. Tan, and C. Jagadish, "The role of intersubband optical transitions on the electrical properties of InGaAs/GaAs quantum dot solar cells," *Prog. Photovolt., Res. Appl.*, vol. 21, no. 4, pp. 736–746, Jun. 2013, doi: 10.1002/pip.2161.

[10] D. Guimard, R. Morihara, D. Bordel, K. Tanabe, Y. Wakayama, M. Nishioka, and Y. Arakawa, "Fabrication of InAs/GaAs quantum dot solar cells with enhanced photocurrent and without degradation of open circuit voltage," *Appl. Phys. Lett.*, vol. 96, no. 20, May 2010, Art. no. 203507, doi: 10.1063/1.3427392.

[11] T. Sugaya, O. Numakami, R. Oshima, S. Furue, H. Komaki, T. Amano, K. Matsubara, Y. Okano, and S. Niki, "Ultra-high stacks of InGaAs/GaAs quantum dots for high efficiency solar cells," *Energy Environ. Sci.*, vol. 5, no. 3, pp. 6233–6237, Feb. 2012, doi: 10.1109/PVSC.2011.6186495.

[12] S. A. Amin, M. T. Hasan, and M. S. Islam, "The effects of interdot spacing and dot size on the performance of InGaAs/GaAs QDIBSC," *Int. J. Photoenergy*, vol. 2017, Oct. 2017, Art. no. 9160381, doi: 10.1155/2017/9160381.

[13] S. A. Amin, M. T. Hasan, and M. S. Islam, "$In_xGa_{1-x}As$/GaAs-based intermediate band solar cell: Effects of quantum dots," in *Proc. IEEE Region Conf. (TENCON)*, Singapore, Nov. 2016, pp. 56–2753, doi: 10.1109/TENCON.2016.7848541.

[14] K. Yoshikawa, H. Kawasaki, W. Yoshida, T. Irie, K. Konishi, K. Nakano, T. Uto, D. Adachi, M. Kanematsu, H. Uzu, and K. Yamamoto, "Silicon heterojunction solar cell with interdigitated back contacts for a photoconversion efficiency over 26%," *Nat. Energy*, vol. 2, Mar. 2017, Art. no. 17032, doi: 10.1038/nenergy.2017.32S.

[15] W. Glunz and F. Feldmann, "SiO_2 surface passivation layers—A key technology for silicon solar cells," *Sol. Energy Mater. Sol. Cells*, vol. 185, pp. 69–260, Oct. 2018, doi: 10.1016/j.solmat.2018.04.029.

[16] R. Bernal-Correa, A. Morales-Acevedo, Á. Pulzara Mora, J. M. Monsalve, and M. L. López, "Design of $Al_xGa_{1-x}As$/GaAs/$InyGa_{1-y}As$ triple junction solar cells with anti-reflective coating," *Mater. Sci. Semicond. Process.*, vol. 37, pp. 57–61, Sep. 2015, doi: 10.1016/j.mssp.2015.01.020.

[17] D. KC, R. Wagle, R. Gaib, A. Shrivastava, and L. N. Mishra, "Modelling and simulation of AlGaAs/GaAs solar cell," *Amer. J. Eng. Res.*, vol. 9, no. 4, pp. 218–223, 2020.

[18] M. Victoria, R. Herrero, C. Domínguez, I. Antón, S. Askins, and G. Sala, "Characterization of the spatial distribution of irradiance and spectrum in concentrating photovoltaic systems and their effect on multi-junction solar cells," *Prog. Photovolt., Res. Appl.*, vol. 21, no. 3, pp. 308–318, May 2013, doi: 10.1002/pip.1183.

[19] P. Moon, K. Park, E. Yoon, and J.-P. Leburton, "Anomalous strain relaxation and light-hole character enhancement in GaAs capped InAs/$In_{0.53}Ga_{0.47}As$ quantum ring," *Phys. Status Solidi RRL, Rapid Res. Lett.*, vol. 3, nos. 2–3, pp. 76–78, Mar. 2009, doi: 10.1002/pssr.200802277.

[20] O. L. Lazarenkova and A. A. Balandin, "Miniband formation in a quantum dot crystal," *J. Appl. Phys.*, vol. 89, no. 10, pp. 5509–5515, May 2001, doi: 10.1063/1.1366662.

[21] (Aug. 30, 2006). *Atlas Users Manual*. Accessed: Sep. 8, 2020. [Online]. Available: https://dynamic.silvaco.com/dynamicweb/jsp/downloads/DownloadManualsAction.do?req=silen-manuals&nm=atlas

[22] X. Lu, R. Hao, M. Diaz, R. L. Opila, and A. Barnett, "Improving GaP solar cell performance by passivating the surface using $Al_xGa_{1-x}P$ epi-layer," *IEEE J. Electron Devices Soc.*, vol. 1, no. 5, pp. 111–116, May 2013, doi: 10.1109/JEDS.2013.2266410.

[23] W. Liang, J. Tong, P. Narangari, S. Armand, T. C. Kho, M. Ernst, D. Walter, S. R. Surve, K. R. McIntosh, M. Stocks, K. J. Weber, A. Blakers, and K. C. Fong, "Impact of al doping on surface passivation of TiO_x on Si," *IEEE J. Photovolt.*, vol. 10, no. 4, pp. 940–944, Jul. 2020, doi: 10.1109/JPHOTOV.2020.2982169.

[24] T. Sertel, Y. Ozen, V. Baran, and S. Ozcelik, "Effect of single-layer Ta_2O_5 and double-layer SiO_2/Ta_2O_5 anti-reflective coatings on GaInP/GaAs/Ge triple-junction solar cell performance," *J. Alloys Compounds*, vol. 806, pp. 439–450, Oct. 2019, doi: 10.1016/j.jallcom.2019.07.257.

[25] *Refractive Index Database*. Accessed: Sep. 8, 2020. [Online]. Available: https://refractiveindex.info/?shelf=other&book=GaAs-InAs&page=Adachi

[26] K. Attari, L. Amhaimar, A. El Yaakoubi, A. Asselman, and M. Bassou, "The design and optimization of GaAs single solar cells using the genetic algorithm and silvaco ATLAS," *Int. J. Photoenergy*, vol. 2017, Nov. 2017, Art. no. 8269358, doi: 10.1155/2017/8269358.

[27] C. G. Bailey, D. V. Forbes, S. J. Polly, Z. S. Bittner, Y. Dai, C. Mackos, R. P. Raffaelle, and S. M. Hubbard, "Open-circuit voltage improvement of InAs/GaAs quantum-dot solar cells using reduced InAs coverage," *IEEE J. Photovolt.*, vol. 2, no. 3, pp. 269–275, Jul. 2012, doi: 10.1109/JPHOTOV.2012.2189047.

[28] B. S. Richards, "Single-material TiO_2 double-layer antireflection coatings," *Sol. Energy Mater. Sol. Cells*, vol. 79, no. 3, pp. 369–390, Sep. 2003, doi: 10.1016/S0927-0248(02)00473-7.

[29] W.-J. Ho, J.-C. Lin, J.-J. Liu, W.-B. Bai, and H.-P. Shiao, "Electrical and optical characterization of sputtered silicon dioxide, indium tin oxide, and silicon dioxide/Indium tin oxide antireflection coating on single-junction GaAs solar cells," *Materials*, vol. 10, no. 7, p. 700, Jun. 2017, doi: 10.3390/ma10070700.

[30] Y.-W. Ok, A. M. Tam, Y.-Y. Huang, V. Yelundur, A. Das, A. M. Payne, V. Chandrasekaran, A. D. Upadhyaya, A. Jain, and A. Rohatgi, "Screen printed, large area bifacial N-type back junction silicon solar cells with selective phosphorus front surface field and boron doped poly-Si/SiO_x passivated rear emitter," *Appl. Phys. Lett.*, vol. 113, no. 26, Dec. 2018, Art. no. 263901, doi: 10.1063/1.5059559.

[31] G. Yang, A. Ingenito, N. van Hameren, O. Isabella, and M. Zeman, "Design and application of ion-implanted polySi passivating contacts for interdigitated back contact c-Si solar cells," *Appl. Phys. Lett.*, vol. 108, Jan. 2016, Art. no. 033903, doi: 10.1063/1.4940364.

[32] Q. Wang, W. Wu, N. Yuan, Y. Li, Y. Zhang, and J. Ding, "Influence of SiOx film thickness on electrical performance and efficiency of TOPCon solar cells," *Sol. Energy Mater. Sol. Cells*, vol. 208, May 2020, Art. no. 110423, doi: 10.1016/j.solmat.2020.110423.

[33] A. Kósa, M. Mikolášek, L. Stuchlíková, L. Harmatha, W. Dawidowski, B. Ściana, and M. Tłaczała, "Electrophysical properties of GaAs P–I–N structures for concentrator solar cell applications," *J. Electr. Eng.*, vol. 67, no. 5, pp. 377–382, Sep. 2016, doi: 10.1515/jee-2016-0054.

[34] A. S. Kushwaha, P. Mahala, and C. Dhanavantri, "Optimization of p-GaN/InGaN/n-GaN double heterojunction p-i-n solar cell for high efficiency: Simulation approach," *Int. J. Photoenergy*, vol. 2014, Apr. 2014, Art. no. 819637, doi: 10.1155/2014/819637.

[35] Y. Shoji, K. Watanabe, and Y. Okada, "Photoabsorption improvement in multi-stacked InGaAs/GaAs quantum dot solar cell with a light scattering rear texture," *Sol. Energy Mater. Sol. Cells*, vol. 204, Jan. 2020, Art. no. 110216, doi: 10.1016/j.solmat.2019.110216.

[36] E. C. Weiner, R. Jakomin, D. N. Micha, H. Xie, P.-Y. Su, L. D. Pinto, M. P. Pires, F. A. Ponce, and P. L. Souza, "Effect of capping procedure on quantum dot morphology: Implications on optical properties and efficiency of InAs/GaAs quantum dot solar cells," *Sol. Energy Mater. Sol. Cells*, vol. 178, pp. 240–248, May 2018, doi: 10.1016/j.solmat.2018.01.028.

[37] M. Li, H. Shen, L. Zhuang, D. Chen, and X. Liang, "SiO2Antireflection coatings fabricated by electron-beam evaporation for black monocrystalline silicon solar cells," *Int. J. Photoenergy*, vol. 2014, May 2014, Art. no. 670438, doi: 10.1155/2014/670438.

[38] D. W. Lee, M. F. Bhopal, S. H. Lee, A. R. Lee, H. J. Kim, M. A. Rehman, Y. Seo, K. Lim, W. Shin, and S. H. Lee, "Effect of additional HfO_2 layer deposition on heterojunction c-Si solar cells," *Energy Sci. Eng.*, vol. 6, no. 6, pp. 706–715, Dec. 2018, doi: 10.1002/ese3.245.

[39] K. Xiong, H. Mi, T.-H. Chang, D. Liu, Z. Xia, M.-Y. Wu, X. Yin, S. Gong, W. Zhou, J. C. Shin, and X. Li, "AlGaAs/Si dual-junction tandem solar cells by epitaxial lift-off and print-transfer-assisted direct bonding," *Energy Sci. Eng.*, vol. 6, no. 1, pp. 47–55, Jan. 2018, doi: 0.1002/ese3.182.

ATIA ISLAM ANKHI received the B.Sc. (Eng.) degree in electrical and electronic engineering from the Khulna University of Engineering & Technology (KUET), in 2020, where she is currently pursuing the M.Sc. (Eng.) degree.

Her research interest includes the next-generation photovoltaic solar cell having high performance.

MD. RAFIQUL ISLAM (Member, IEEE) received the B.Sc. (Eng.) degree in electrical and electronic engineering from the Bangladesh University of Engineering and Technology (BUET), Dhaka, Bangladesh, in 1998, the M.Sc. (Eng.) degree in electrical and electronic engineering from the Khulna University of Engineering & Technology (KUET), Khulna, Bangladesh, in 2006, and the Ph.D. degree in semiconductor device growth, characterization, and fabrication from the University of Fukui, Japan, in 2010.

He is currently working as a Professor with the Khulna University of Engineering & Technology. He has published over 90 research papers in national and international conferences and journals. His research interests include thin films solar cells, growth characterization and fabrications, advanced semiconductor materials properties, and compound semiconductor-based devices. He received the Monbukagakusho Scholarship (MEXT Scholarship), Japan, from 2007 to 2010. His two papers received the best paper award at international conferences.

MD. TANVIR HASAN (Member, IEEE) received the B.Sc. and M.Sc. degrees in electrical and electronic engineering from the Khulna University of Engineering & Technology (KUET), Bangladesh, in 2006 and 2007, respectively, and the Ph.D. degree in electrical and electronic engineering from the Graduate School of Engineering, University of Fukui, Japan, in 2013.

He is currently working as an Associate Professor with the Department of Electrical and Electronic Engineering, Jashore University of Science and Technology (JUST), Bangladesh. His research interests include growth, design, fabrication, characterization, simulation, and modeling of III-V-based semiconductor devices (Electronic and Optoelectronic). He is the author or coauthor of more than 50 research papers in conferences and journals. He received the Monbukagakusho (MEXT) Scholarship, Japan, from 2010 to 2013. He received the IEEE Student Paper Award (Honorary Mentioned) from the IEEE Electron Devices Society, Bangladesh Chapter, in 2007. He has been a member of IEEE Electron Devices Society, since 2008. He served as a Secretary as IEEE Young Professional for Bangladesh Section (BDS), and an Executive Committee Member as Professional Activity Coordinator for IEEE BDS, in 2016 and 2017. He serves as a Reviewer for IEEE TRANSACTIONS ON ELECTRON DEVICES, *Journal of Applied Physics*, and *Applied Physics Letters*.

EKLAS HOSSAIN (Senior Member, IEEE) received the B.S. degree in electrical and electronic engineering from the Khulna University of Engineering & Technology, Bangladesh, in 2006, the M.S. degree in mechatronics and robotics engineering from International Islamic University Malaysia, Malaysia, in 2010, and the Ph.D. degree from the College of Engineering and Applied Science, University of Wisconsin Milwaukee (UWM). He has been involved with several research projects on renewable energy and grid tied microgrid system at Oregon Tech, as an Assistant Professor with the Department of Electrical Engineering and Renewable Energy, since 2015. He is working as an Associate Researcher with the Oregon Renewable Energy Center (OREC). He has been working in the area of distributed power systems and renewable energy integration for last ten years, and he has published a number of research papers and posters in this field. His research interests include modeling, analysis, design, and control of power electronic devices, energy storage systems, renewable energy sources, integration of distributed generation systems, microgrid and smart grid applications, robotics, and advanced control systems. He and his dedicated research team is looking forward to exploring methods to make the electric power systems more sustainable, cost-effective, and secure through extensive research and analysis on energy storage, microgrid system, and renewable energy sources. He is a Senior Member of the Association of Energy Engineers (AEE). He is a registered Professional Engineer (PE) in the State of Oregon, USA. He is also a Certified Energy Manager (CEM) and Renewable Energy Professional (REP). He is the winner of the Rising Faculty Scholar Award from the Oregon Institute of Technology, in 2019, for his outstanding contribution in teaching. He is currently serving as an Associate Editor for IEEE ACCESS.